Use of Classical Plate Finite Elements for the Analysis of Electroactive Composite Plates. Numerical Validations

F. Pablo, Isabelle Bruant, Olivier Polit

Use of Classical Plate Finite Elements for the Analysis of Electroactive Composite Plates. Numerical Validations

F. PABLO,* I. BRUANT AND O. POLIT

Laboratoire de Mécanique de Paris X (LMpX), Paris X University, 50 rue de Sèvres 92410 Ville d'Avray, France

ABSTRACT: An original piezoelectric plate theory has been presented in the companion paper (Osmont and Pablo, 2008). The particularity of the 'piezoelectric', finite element stemming from this theory lies in the fact that no electric degree of freedom is needed to take into account the electromechanical coupling. This article is focused on the validation of this theory through various benchmarks issued from literature. It will be proved that results are in quite agreement with static and dynamic reference solutions of laminated composite plates equipped with piezoelectric patches.

Key Words: piezoelectric, plate finite element, *a priori* assumptions, no electric degree of freedom.

INTRODUCTION

THE purpose of the present studies is to perform active vibration control of composite panels using distributed electro-active actuators and sensors. Many previous works proved that the number and location of actuator/sensor pairs have a great influence on control efficiency (see, for example, (Preumont, 1997)). As the actuators need to be perfectly bonded to the controlled structure in order to maximize the electromechanical interactions, patches locations have to be defined using numerical simulations previous to any experimental application.

From this point of view, the present work is focused on modeling laminated composite plates equipped with piezoelectric patches for active vibration control applications. A new methodology has been presented in the companion paper (Osmont and Pablo, 2008) to analyze such electro-mechanically coupled problems using classical mechanical plate finite elements.

Indeed, based on *a priori* assumptions, it has been shown that electric variables could analytically be eliminated from the problem unknowns. The piezoelectric effects are then taken into account via external forces depending on electric boundary conditions and modified elastic coefficients.

This article presents a numerical validation of this original theory through various benchmarks issued from literature. The benchmark selection proposed here was limited by the need of piezoelectric electromechanical properties to be fully known in order to implement the present theory. As these properties are generally incomplete in the open literature, other interesting benchmarks could not be used for results comparisons.

The present work efficiency is hereafter proved through comparisons with various finite element theories with, or without, electric degrees of freedom. In particular, the present merely elastic model (i.e., without electric degree of freedom) is compared to reference piezoelectric finite elements including electric degrees of freedom and proposed by Bruant and Polit (2004) and Polit and Bruant (2005).

The article is organized as follows. To stand with, main results obtained by Osmont and Pablo (2008) are reminded in the section 'Main Theoretical Results'. The finite element implementation of the present theory is then developed in the section 'Finite Element Considerations'.

Finally, various benchmarks are proposed so as to evaluate the present theory for thin plates made of – or including – piezoelectric layers submitted to static electromechanical loads and modal analysis. In particular, the last benchmark leads to a discussion concerning the appropriate way to take into account the isolated electric boundary conditions.

NOTATIONS

In following developments, latin indices $i, j, \ldots,$ take their values in the set $\{1,2,3\}$ while greek indices $\alpha, \beta, \ldots,$ take their values in the set $\{1, 2\}$.

*Author to whom correspondence should be addressed.
E-mail: frederic.pablo@u-paris10.fr

Einstein agreement stating the summation on repeated indices and the classic notation $(\ )_{,\alpha} = \partial(\ )/\partial x_\alpha$ are used. Moreover, classical engineering notations are used for stresses and strains.

The following notations are generally used:

- double bar symbols, such as $\mathbb{A}$, denote tensors of order greater than two,
- bold symbols, such as $\mathbf{A}$, denote vectors and matrices,
- regular symbols, such as A, denote scalars,
- the t superscript denotes the transpose,
- the d superscript denotes prescribed values (given boundary conditions),
- the E superscript denotes the short-circuited (closed-circuit) variables,
- the D superscript denotes the isolated (open-circuit) variables,
- the S superscript denotes the strain-free variables,
- the T superscript denotes the stress-free variables.

Finally, the following notations will in particular represent:

$\mathbf{u} = (u_1\ u_2\ u_3)^t$: Mechanical displacement vector
$\ddot{\mathbf{u}} = (\ddot{u}_1\ \ddot{u}_2\ \ddot{u}_3)^t$: Acceleration vector
$\mathbf{f}^d = (f_1^d\ f_2^d\ f_3^d)^t$: Applied body forces
$\mathbf{F}^d = (F_1^d\ F_2^d\ F_3^d)^t$: Applied surface forces
$\mathbf{n} = (n_1\ n_2\ n_3)^t$: Normal vector
$\mathbf{S} = (S_{11}\ S_{22}\ S_{33}\ 2S_{13}\ 2S_{23}\ 2S_{12})^t$: Strain vector
$\mathbf{S}^p = (S_{11}\ S_{22}\ 2S_{12})^t$: In-plane strain vector
$\mathbf{S}^s\ (2S_{13}\ 2S_{23})^t$: Transverse shear strain vector
$\mathbf{T} = (T_{11}\ T_{22}\ T_{33}\ T_{13}\ T_{23}\ T_{12})^t$: Stress vector
$\mathbf{D} = (D_1\ D_2\ D_3)^t$: Electric displacement vector
$\mathbf{E} = (E_1\ E_2\ E_3)^t$: Electric field vector
Φ: Electric potential
Q^d: Surface electric charges
q^d: Body electric charges
$\mathbb{S}$: Compliance tensor (fourth order)
$\mathbb{C}$: Stiffness tensor (fourth order)
$\mathbb{e}$ and $\mathbb{h}$: Strain-free piezoelectric tensors (third order)
$\mathbb{d}$ and $\mathbb{g}$: Stress-free piezoelectric tensors (third order)
ε: Dielectric tensor (second order)
β: Susceptibility tensor (second order)

MAIN THEORETICAL RESULTS

Based on *a priori* plate assumption, it has been proven that the in-plane stresses can be expressed as a linear function of membrane and bending strains for all possible electric boundary conditions defined at the layers' top and bottom surfaces of piezoelectric actuators. Assuming each layer to be homogeneous, the following relationships have been established depending on the electric boundary conditions at its top and bottom surfaces:

Case 1: electric charges (Q_l^d and Q_u^d) are known on the two surfaces of the i*th* layer

$$T_{\alpha\beta}^i = \overline{\mathbb{C}}_{\alpha\beta\gamma\delta}^{Di}\, S_{\gamma\delta}^0 + z\, \overline{\mathbb{C}}_{\alpha\beta\gamma\delta}^{Di}\, R_{\gamma\delta}^1 - \overline{\mathbb{h}}_{\alpha\beta 3}^{ti}\, Q_l^d \tag{1}$$

Case 2: electric charges (Q_l^d) and electric potential (Φ_u^d) are, respectively, known on the lower and upper surfaces of the i*th* layer

$$T_{\alpha\beta}^i = \overline{\mathbb{C}}_{\alpha\beta\gamma\delta}^{Di}\, S_{\gamma\delta}^0 + z\, \overline{\mathbb{C}}_{\alpha\beta\gamma\delta}^{Di}\, R_{\gamma\delta}^1 - \overline{\mathbb{h}}_{\alpha\beta 3}^{ti}\, Q_l^d \tag{2}$$

Case 3: electric potential (Φ_l^d) and electric charges (Q_u^d) are, respectively, known on the lower and upper surfaces of the i*th* layer

$$T_{\alpha\beta}^i = \overline{\mathbb{C}}_{\alpha\beta\gamma\delta}^{Di}\, S_{\gamma\delta}^0 + z\, \overline{\mathbb{C}}_{\alpha\beta\gamma\delta}^{Di}\, R_{\gamma\delta}^1 - \overline{\mathbb{h}}_{\alpha\beta 3}^{ti}\, Q_u^d \tag{3}$$

Case 4: electric potentials (Φ_l^d and Φ_u^d) are, respectively, known on both surfaces of the i*th* layer

$$T_{\alpha\beta}^i = \overline{\mathbb{C}}_{\alpha\beta\gamma\delta}^{Ei}\, S_{\gamma\delta}^0 + (z\, \overline{\mathbb{C}}_{\alpha\beta\gamma\delta}^{Di} - z_{mid}^i\, \overline{\mathbb{h}}_{\alpha\beta 3}^{ti}\, \overline{\mathbb{e}}_{3\gamma\delta}^i)\, R_{\gamma\delta}^1 + \overline{\mathbb{h}}_{\alpha\beta 3}^{ti}\, \overline{\varepsilon}_{33}^{Si}\, \frac{\Phi_u^d - \Phi_l^d}{h^i}, \tag{4}$$

where $\mathbf{S}^0$ and $\mathbf{R}^1$ are respectively the in-plane strains deriving from membrane and bending distortion. They are independent of z.

Finally, thick plates shearing behavior is given by:

$$T_{\alpha 3} = \overline{\mathbb{C}}_{\alpha 3\gamma 3}^{D}\, S_{\gamma 3} \tag{5}$$

FINITE ELEMENT CONSIDERATIONS

Taking into account these theoretical results, the variational formulation of the boundary value problem can be written as follows:

Find $\mathbf{u}(M, t), \mathbf{T}(M, t)$ such that they meet:
$\forall\, t \in\ ]0, T[$,
$\forall\ \overset{*}{\mathbf{u}} \in \mathcal{U}_u^0,\ \mathcal{U}_u^0 = \{\overset{*}{\mathbf{u}}(M) | \overset{*}{\mathbf{u}}(M) = 0 \text{ on } \Gamma_u,\ \overset{*}{\mathbf{u}} \text{ regular}\}$,
the dynamic equation:

$$\int_\Omega \overset{*}{\mathbf{S}}{}^t(\overset{*}{\mathbf{u}})\, \mathbf{T}(\mathbf{u})\, \mathrm{d}\Omega + \int_\Omega \overset{*}{\mathbf{u}}{}^t\, \mathbf{f}^d\, \mathrm{d}\Omega + \int_{\Gamma_F} \overset{*}{\mathbf{u}}{}^t\, \mathbf{F}^d\, \mathrm{d}S - \int_\Omega \rho\, \overset{*}{\mathbf{u}}{}^t\, \ddot{\mathbf{u}}\, \mathrm{d}\Omega = 0, \tag{6}$$

the layers' electromechanical constitutive equations:

$$\begin{cases} T^i_{\alpha\beta} = (\overline{\mathbb{C}}^{Di}_{\alpha\beta\gamma\delta} - \overline{\mathbb{h}}^{ti}_{\alpha\beta3}\,\Psi^{0Di}_{3\gamma\delta})\,S^0_{\gamma\delta} + (z\,\overline{\mathbb{C}}^{Di}_{\alpha\beta\gamma\delta} - \overline{\mathbb{h}}^{ti}_{\alpha\beta3}\,\Psi^{1Di}_{3\gamma\delta}) \\ \qquad R^1_{\gamma\delta} - \overline{\mathbb{h}}^{ti}_{\alpha\beta3}\,D^{bound}_3, \\ T^i_{\alpha3} = \overline{\mathbb{C}}^{Di}_{\alpha3\gamma3}\,S_{\gamma3}, \end{cases} \tag{7}$$

the mechanical displacement boundary conditions:

$$u_i = u_i^d \quad \text{on} \quad \Gamma_u \Leftrightarrow \mathbf{u} \in \mathcal{U}^0_u, \tag{8}$$

in which Ψ^{0Di} and Ψ^{1Di} are zero for cases 1, 2, 3 (recalled above), and are equal to:

$$\Psi^{kDi} = \frac{\displaystyle\int_{z^i_l}^{z^i_u} z^k\,\overline{\mathbb{h}}_{3\gamma\delta}\,\mathrm{d}z}{\displaystyle\int_{z^i_l}^{z^i_u} \overline{\beta}^S_{33}}\,\mathrm{d}z, \quad k = 0, 1, \quad \text{for case 4.}$$

The developments presented hereafter are obtained assuming the electro-active layers to be homogeneous and voltage driven. These electric boundary conditions correspond to case 4, mentioned in the section 'Main Theoretical Results'. in this case, the general in-plane behavior (first equation of (7)) is replaced by Equation (4).

Moreover, mechanical layers (non-electro-active ones) behavior will hereafter be characterized by the following in-plane and shearing constitutive laws:

$$T^i_{\alpha\beta}(\mathbf{u}) = \overline{\mathbb{C}}^{i}_{\alpha\beta\gamma\delta}\,S^0\gamma\delta(\mathbf{u})_+ z\,\overline{\mathbb{C}}^{i}_{\alpha\beta\gamma\delta}\,R^1_{\gamma\delta}(\mathbf{u}), \tag{9}$$

$$T^i_{\alpha3}(\mathbf{u}) = \overline{\mathbb{C}}^{\,i}_{\alpha3\gamma3}\,S_{\gamma3}(\mathbf{u}). \tag{10}$$

Finally, it is assumed that the laminate plate is made of N layers of which N_p layers are electro-active actuators.

Let us now estimate the strain energy given by the first term of the left-hand side in Equation (6). As presented in the companion paper (Osmont and Pablo, 2008), in-plane strains can be written as a linear function of the membrane and bending strains:

$$S_{\alpha\beta}(\mathbf{u}) = S^0_{\alpha\beta}(\mathbf{u}) + z\,R^1_{\alpha\beta}(\mathbf{u}). \tag{11}$$

introducing Equations (11) and (4) in the strain energy expression, we obtain:

$$\begin{aligned} \int_\Omega \overset{*}{\mathbf{S}}{}^t\,\mathbf{T}\,\mathrm{d}\Omega &= \int_\Sigma \overset{*}{S}{}^{0t}{}_{\alpha\beta}\left\{\sum_{i=1}^{N_p}\left(\int_{z^i_l}^{z^i_u}\overline{\mathbb{C}}^{Ei}_{\alpha\beta\gamma\delta}\,\mathrm{d}z\right) + \sum_{i=1}^{N-N_p}\left(\int_{z^i_l}^{z^i_u}\overline{\mathbb{C}}^{i}_{\alpha\beta\gamma\delta}\,\mathrm{d}z\right)\right\}S^0_{\gamma\delta}\,\mathrm{d}S \\ &+ \int_\Sigma \overset{*}{S}{}^{0t}{}_{\alpha\beta}\left\{\sum_{i=1}^{N_p}\left[\int_{z^i_l}^{z^i_u}\left(z\,\overline{\mathbb{C}}^{Di}_{\alpha\beta\gamma\delta} - z^i_{mid}\,\overline{\mathbb{h}}^{ti}_{\alpha\beta3}\,\overline{\mathbb{e}}^{i}_{3\gamma\delta}\right)\mathrm{d}z\right] + \sum_{i=1}^{N-N_p}\left(\int_{z^i_l}^{z^i_u} z\,\overline{\mathbb{C}}^{i}_{\alpha\beta\gamma\delta}\,\mathrm{d}z\right)\right\}R^1_{\gamma\delta}\,\mathrm{d}S \\ &+ \int_\Sigma \overset{*}{R}{}^{1t}{}_{\alpha\beta}\left\{\sum_{i=1}^{N_p}\left(\int_{z^i_l}^{z^i_u} z\,\overline{\mathbb{C}}^{Ei}_{\alpha\beta\gamma\delta}\,\mathrm{d}z\right) + \sum_{i=1}^{N-N_p}\left(\int_{z^i_l}^{z^i_u} z\overline{\mathbb{C}}^{i}_{\alpha\beta\gamma\delta}\,\mathrm{d}z\right)\right\}S^0_{\gamma\delta}\,\mathrm{d}S \\ &+ \int_\Sigma \overset{*}{R}{}^{1t}{}_{\alpha\beta}\left\{\sum_{i=1}^{N_p}\int_{z^i_l}^{z^i_u}\left(z^2\,\overline{\mathbb{C}}^{Di}_{\alpha\beta\gamma\delta} - z\,z^i_{mid}\,\overline{\mathbb{h}}^{ti}_{\alpha\beta3}\,\overline{\mathbb{e}}^{i}_{3\gamma\delta}\right)\mathrm{d}z + \sum_{i=1}^{N-N_p}\left(\int_{z^i_l}^{z^i_u} z^2\,\overline{\mathbb{C}}^{i}_{\alpha\beta\gamma\delta}\,\mathrm{d}z\right)\right\}R^1_{\gamma\delta}\mathrm{d}S \\ &+ \int_\Sigma \overset{*}{S}{}^{t}{}_{\alpha3}\left\{\sum_{i=1}^{N_p}\left(\int_{z^i_l}^{z^i_u}\overline{\mathbb{C}}^{Di}_{\alpha3\gamma3}\,\mathrm{d}z\right) + \sum_{i=1}^{N-N_p}\left(\int_{z^i_l}^{z^i_u}\overline{\mathbb{C}}^{i}_{\alpha3\gamma3}\,\mathrm{d}z\right)\right\}S_{\alpha3}\,\mathrm{d}S \\ &+ \int_\Sigma\left\{\overset{*}{S}{}^{0t}{}_{\alpha\beta}\sum_{i=1}^{N_p}\left[\int_{z^i_l}^{z^i_u}\overline{\mathbb{h}}^{ti}_{\alpha\beta3}\,\overline{\mathbb{e}}^{Si}_{33}\,\frac{\Phi^d_u - \Phi^d_l}{h^i}\,\mathrm{d}z\right] + {}^t\overset{*}{R}{}^{1}{}_{\alpha\beta}\sum_{i=1}^{N_p}\left[\int_{z^i_l}^{z^i_u} z\,{}^t\overline{\mathbb{h}}^{i}_{\alpha\beta3}\,\overline{\mathbb{e}}^{Si}_{33}\,\frac{\Phi^d_u - \Phi^d_l}{h^i}\,\mathrm{d}z\right]\right\}\mathrm{d}S, \end{aligned}$$

Integrations with respect to the thickness are performed and the following expression is deduced:

$$\begin{aligned} \int_\Omega \overset{*}{\mathbf{S}}{}^t\,\mathbf{T}\,\mathrm{d}\Omega &= \int_\Sigma \overset{*}{S}{}^{0t}{}_{\alpha\beta}\left\{\sum_{i=1}^{N_p} h^i\,\overline{\mathbb{C}}^{Ei}_{\alpha\beta\gamma\delta} + \sum_{i=1}^{N-N_p} h^i\,\overline{\mathbb{C}}^{i}_{\alpha\beta\gamma\delta}\right\}S^0_{\gamma\delta}\,\mathrm{d}S \\ &+ \int_\Sigma \overset{*}{S}{}^{0t}{}_{\alpha\beta}\left\{\sum_{i=1}^{N_p} z^i_{mid}\,h^i\left(\overline{\mathbb{C}}^{Di}_{\alpha\beta\gamma\delta} - \overline{\mathbb{h}}^{ti}_{\alpha\beta3}\,\overline{\mathbb{e}}^{i}_{3\gamma\delta}\right) + \sum_{i=1}^{N-N_p} z^i_{mid}\,h^i\,\overline{\mathbb{C}}^{i}_{\alpha\beta\gamma\delta}\right\}R^1_{\gamma\delta}\,\mathrm{d}S \\ &+ \int_\Sigma \overset{*}{R}{}^{1t}{}_{\alpha\beta}\left\{\sum_{i=1}^{N_p} z^i_{mid}\,h^i\,\overline{\mathbb{C}}^{Ei}_{\alpha\beta\gamma\delta} + \sum_{i=1}^{N-N_p} z^i_{mid}\,h^i\,\overline{\mathbb{C}}^{i}_{\alpha\beta\gamma\delta}\right\}S^0_{\gamma\delta}\,\mathrm{d}S \\ &+ \int_\Sigma \overset{*}{R}{}^{1t}{}_{\alpha\beta}\left\{\sum_{i=1}^{N_p}\left[\frac{(z^i_u)^3 - (z^i_l)^3}{3}\,\overline{\mathbb{C}}^{Di}_{\alpha\beta\gamma\delta} - (z^i_{mid})^2 h^i\,\overline{\mathbb{h}}^{ti}_{\alpha\beta3}\,\overline{\mathbb{e}}^{i}_{3\gamma\delta}\right] + \sum_{i=1}^{N-N_p}\frac{(z^i_u)^3 - (z^i_l)^3}{3}\,\overline{\mathbb{C}}^{i}_{\alpha\beta\gamma\delta}\right\}R^1_{\gamma\delta}\,\mathrm{d}S \end{aligned}$$

$$+\int_\Sigma \overset{*}{S}{}^t{}_{\alpha 3}\left\{\sum_{i=1}^{N_p} h^i\,\overline{\mathbb{C}}^{Di}_{3\alpha 3\gamma}+\sum_{i=1}^{N-N_p} h^i\,\overline{\mathbb{C}}^{i}_{3\alpha 3\gamma}\right\}S_{\gamma 3}\,\mathrm{d}S$$
$$+\int_\Sigma \overset{*}{S}{}^{0t}{}_{\alpha\beta}\left\{\sum_{i=1}^{N_p}\left[\overline{\mathbb{h}}^{ti}_{\alpha\beta 3}\,\overline{\varepsilon}^{Si}_{33}\left(\Phi^d_u-\Phi^d_l\right)\right]\right\}\mathrm{d}S$$
$$+\int_\Sigma \overset{*}{R}{}^{1t}{}_{\alpha\beta}\left\{\sum_{i=1}^{N_p}\left[z^i_{mid}\,\overline{\mathbb{h}}^{ti}_{\alpha\beta 3}\,\overline{\varepsilon}^{Si}_{33}\left(\Phi^d_u-\Phi^d_l\right)\right]\right\}\mathrm{d}S.$$

Now, it is possible to show that (see for example (Ikeda, 1990)):

$$\overline{\mathbb{C}}^{Di}_{\alpha\beta\gamma\delta}-\overline{\mathbb{h}}^{ti}_{\alpha\beta 3}\,\overline{\mathbb{e}}^{i}_{3\gamma\delta}=\overline{\mathbb{C}}^{Ei}_{\alpha\beta\gamma\delta} \tag{12}$$

As a consequence, the second term can be simplified and the following results obtained:

$$\int_\Omega \overset{*}{\mathbf{S}}{}^t\,\mathbf{T}\,\mathrm{d}\Omega$$
$$=\int_\Sigma \overset{*}{S}{}^{0t}{}_{\alpha\beta}\underbrace{\left\{\sum_{i=1}^{N_p}h^i\overline{\mathbb{C}}^{Ei}_{\alpha\beta\gamma\delta}+\sum_{i=1}^{N-N_p}h^i\overline{\mathbb{C}}^{i}_{\alpha\beta\gamma\delta}\right\}}_{\mathbb{K}_1}S^0_{\gamma\delta}\,\mathrm{d}S$$
$$+\int_\Sigma \overset{*}{S}{}^{0t}{}_{\alpha\beta}\underbrace{\left\{\sum_{i=1}^{N_p}z^i_{mid}h^i\overline{\mathbb{C}}^{Ei}_{\alpha\beta\gamma\delta}+\sum_{i=1}^{N-N_p}z^i_{mid}h^i\overline{\mathbb{C}}^{i}_{\alpha\beta\gamma\delta}\right\}}_{\mathbb{K}_2}R^1_{\gamma\delta}\,\mathrm{d}S$$
$$+\int_\Sigma \overset{*}{R}{}^{1t}{}_{\alpha\beta}\underbrace{\left\{\sum_{i=1}^{N_p}z^i_{mid}h^i\overline{\mathbb{C}}^{Ei}_{\alpha\beta\gamma\delta}+\sum_{i=1}^{N-N_p}z^i_{mid}h^i\overline{\mathbb{C}}^{i}_{\alpha\beta\gamma\delta}\right\}}_{\mathbb{K}_2}S^0_{\gamma\delta}\,\mathrm{d}S$$
$$+\int_\Sigma \overset{*}{R}{}^{1t}{}_{\alpha\beta}\underbrace{\left\{\sum_{i=1}^{N_p}\left[\frac{(z^i_u)^3-(z^i_l)^3}{3}\overline{\mathbb{C}}^{Di}_{\alpha\beta\gamma\delta}-(z^i_{mid})^2h^i\overline{\mathbb{h}}^{ti}_{\alpha\beta 3}\overline{\mathbb{e}}^{i}_{3\gamma\delta}\right]\right\}}_{\mathbb{K}_3}R^1_{\gamma\delta}\,\mathrm{d}S$$
$$+\int_\Sigma \overset{*}{R}{}^{1t}{}_{\alpha\beta}\underbrace{\left\{\sum_{i=1}^{N-N_p}\frac{(z^i_u)^3-(z^i_l)^3}{3}\overline{\mathbb{C}}^{i}_{\alpha\beta\gamma\delta}\right\}}_{\mathbb{K}_{3'}}R^1_{\gamma\delta}\,\mathrm{d}S$$
$$+\int_\Sigma \overset{*}{S}{}^{t}{}_{\alpha 3}\underbrace{\left\{\sum_{i=1}^{N_p}h^i\overline{\mathbb{C}}^{Di}_{3\alpha 3\gamma}+\sum_{i=1}^{N-N_p}h^i\overline{\mathbb{C}}^{i}_{3\alpha 3\gamma}\right\}}_{\mathbb{K}_4}S_{\gamma 3}\,\mathrm{d}S$$
$$+\int_\Sigma \overset{*}{S}{}^{0t}{}_{\alpha\beta}\underbrace{\left\{\sum_{i=1}^{N_p}\overline{\mathbb{h}}^{ti}_{\alpha\beta 3}\,\overline{\varepsilon}^{Si}_{33}\left(\Phi^d_u-\Phi^d_l\right)\right\}}_{\mathbb{K}_5}\mathrm{d}S$$
$$+\int_\Sigma \overset{*}{R}{}^{1t}{}_{\alpha\beta}\underbrace{\left\{\sum_{i=1}^{N_p}z^i_{mid}\,\overline{\mathbb{h}}^{ti}_{\alpha\beta 3}\,\overline{\varepsilon}^{Si}_{33}\left(\Phi^d_u-\Phi^d_l\right)\right\}}_{\mathbb{K}_6}\mathrm{d}S.$$

Following classical finite element techniques, strains can be expressed with respect to the elementary vector of degrees of freedom (dof) $\mathbf{q_e}$:

$$\mathbf{S}^0=\mathbb{B}_{\mathbf{S}^0}\,\mathbf{q_e}\quad\text{and}\quad\overset{*}{\mathbf{S}}{}^0=\mathbb{B}_{\mathbf{S}^0}\,\overset{*}{\mathbf{q}}_{\mathbf{e}}$$
$$\mathbf{R}^1=\mathbb{B}_{\mathbf{R}^1}\,\mathbf{q_e}\quad\text{and}\quad\overset{*}{\mathbf{R}}{}^1=\mathbb{B}_{\mathbf{R}^1}\,\overset{*}{\mathbf{q}}_{\mathbf{e}}$$
$$\mathbf{S}^s=\mathbb{B}_C\,\mathbf{q_e}\quad\text{and}\quad\overset{*}{\mathbf{S}}{}^s=\mathbb{B}_C\,\overset{*}{\mathbf{q}}_{\mathbf{e}},$$

in which $\mathbb{B}_{\mathbf{S}^0}$, $\mathbb{B}_{\mathbf{R}^1}$, and $\mathbb{B}_C$ are the interpolation matrices for membrane, bending, and transverse shearing strains, respectively.

The internal energy can then be written as follows:

$$\int_\Omega \overset{*}{\mathbf{S}}{}^t\,\mathbf{T}\,\mathrm{d}\Omega=\overset{*}{\mathbf{q}}_{\mathbf{e}}{}^t\underbrace{\int_\Sigma \mathbb{B}^t_{\mathbf{S}^0}\,\mathbb{K}_1\,\mathbb{B}_{\mathbf{S}^0}\,\mathrm{d}S}_{\mathbb{A}}\mathbf{q_e}$$
$$+\overset{*}{\mathbf{q}}_{\mathbf{e}}{}^t\underbrace{\int_\Sigma \mathbb{B}^t_{\mathbf{S}^0}\,\mathbb{K}_2\,\mathbb{B}_{\mathbf{R}^1}\,\mathrm{d}S}_{\mathbb{B}}\mathbf{q_e}$$
$$+\overset{*}{\mathbf{q}}_{\mathbf{e}}{}^t\underbrace{\int_\Sigma \mathbb{B}^t_{\mathbf{R}^1}\,\mathbb{K}_2\,\mathbb{B}_{\mathbf{S}^0}\,\mathrm{d}S}_{\mathbb{B}^t}\mathbf{q_e}$$
$$+\overset{*}{\mathbf{q}}_{\mathbf{e}}{}^t\underbrace{\int_\Sigma \mathbb{B}^t_{\mathbf{R}^1}\left(\mathbb{K}_3+\mathbb{K}_{3'}\right)\mathbb{B}_{\mathbf{R}^1}\mathrm{d}S}_{\mathbb{D}}\mathbf{q_e}$$
$$+\overset{*}{\mathbf{q}}_{\mathbf{e}}{}^t\underbrace{\int_\Sigma \mathbb{B}^t_C\,\mathbb{K}_4\,\mathbb{B}_C\mathbf{S}_C\,\mathrm{d}S}_{\mathbb{E}}\mathbf{q_e}$$
$$+\overset{*}{\mathbf{q}}_{\mathbf{e}}{}^t\underbrace{\int_\Sigma \mathbb{B}^t_{\mathbf{S}^0}\,\mathbb{K}_5\,\mathrm{d}S}_{\mathbf{F}}\mathbf{q_e}$$
$$+\overset{*}{\mathbf{q}}_{\mathbf{e}}{}^t\underbrace{\int_\Sigma \mathbb{B}^t_{\mathbf{R}^1}\,\mathbb{K}_6\,\mathrm{d}S}_{\mathbf{G}}\mathbf{q_e}.$$

$\overline{\mathbb{C}}^{Ei}_{\alpha\beta\gamma\delta}$ and $\overline{\mathbb{C}}^{i}_{\alpha\beta\gamma\delta}$ being symmetric sub-matrices, $\mathbb{K}_2$ is also symmetric. As a consequence, the third term of this last equation is the transpose of the second one.

The modified stiffness matrix and the piezoelectric load vector can then be written as follows:

$$\mathbb{K}=\begin{bmatrix}\mathbb{A}&\mathbb{B}&0\\ \mathbb{B}^t&\mathbb{D}&0\\ 0&0&\mathbb{E}\end{bmatrix}\quad\text{and}\quad\mathbf{F}^{piez}=\begin{pmatrix}\mathbf{F}\\ \mathbf{G}\\ 0\end{pmatrix}, \tag{13}$$

in which $\mathbb{A}$, $\mathbb{B}$, $\mathbb{D}$, and $\mathbb{E}$ sub-matrices and $\mathbf{F}$ and $\mathbf{G}$ sub-vectors are obtained from the short-circuited stiffness matrix ($\mathbb{C}^E$), the isolated stiffness matrix ($\mathbb{C}^D$), the strain-free piezoelectric matrices ($\mathbb{e}$ and $\mathbb{h}$) and the strain-free dielectric matrix (ε^S).

It is to be underlined that Young's moduli E_i, Poisson's ratios ν_{ij}, shear moduli G_{ij}, stress-free piezoelectric constants $\mathbb{d}_{ij}$ and stress-free electric permittivities ε^T are generally the electro-mechanical characteristics provided by manufacturers. Matrices needed for the present model

have thus to be evaluated from these data. This is possible through relationships presented in Ref. (Osmont and Pablo, 2008) (Equation (24)).

Note that the stiffness matrix is still symmetric despite the introduction of the piezoelectric effect. As a consequence, classical numerical methods can be used to solve the electromechanical problem.

Finally, calculating the mass matrix and the mechanical load vectors, the finite element problem to be solved is written as follows:

$$\mathbb{M}\,\ddot{\mathbf{q}}_{\mathbf{e}} + \mathbb{K}\,\mathbf{q}_{\mathbf{e}} + \mathbf{F}^{mech} + \mathbf{F}^{piez} = 0 \qquad (14)$$

Developments presented above have been obtained assuming the piezoelectric layers to be voltage driven by referring to the case 4 of electric boundary conditions (Equation (4)). Similar expressions with modified stiffness matrices and piezoelectric load vectors have been obtained for others electric boundary conditions (cases 1, 2, 3).

NUMERICAL VALIDATIONS

This section aims at evaluating the theory developed in the companion paper (Osmont and Pablo, 2008) using classical mechanical plate finite elements. Five benchmarks, taken from literature, are hereafter examined. First, three benchmarks dealing with plates under static loads are studied:

- A piezoelectric bimorph beam so as to validate the ability of the theory to simulate the behavior of static piezoelectric actuators.
- A cantilever laminate plate so as to validate the electromechanical behavior of composite plates including piezoelectric layers.
- An active plate so as to validate the contribution of piezoelectric patches bounded on purely mechanical plates.

Then, two benchmarks focused on frequency tests are presented:

- A cantilever composite plate including short-circuited piezoelectric layers so as to validate the natural frequencies estimation.
- A simply supported square plate including piezoelectric layers submitted to various electrical boundary conditions which will lead to a discussion on the modeling of these boundary conditions.

Finite Element Considerations

The electro-active plate theory, proposed in the companion paper (Osmont and Pablo, 2008), has been implemented in EvalEF, a Finite Element Software developed for finite element evaluation. This implementation uses the CL8 plate finite element which has been first introduced by Polit et al. (1994).

This element is a classical mechanical eight-node quadrilateral finite element with five degrees of freedom per node (three displacement components and two rotations), based on the Reissner–Mindlin plate model and the field compatibility conditions. This element does not suffer from any numerical pathologies in the field of finite elements: shear locking, membrane locking, spurious modes, etc. (Polit et al., 1994; Ganapathi et al., 1996).

The present evaluations are hereafter compared with results from literature and with an LMpX previous work (Bruant and Polit, 2004) about piezoelectric finite elements with electric degrees of freedom. This last work led to the conception of CL8-based finite elements, in which the electric potential is approximated using the layerwise approach. An evaluation has been performed in order to assess the best compromise between minimum number of degrees of freedom and maximum efficiency. On the one hand, two kinds of finite element approximations for the electric potential with respect to thickness coordinate have been studied: a linear variation and a quadratic variation in each layer. On the other hand, the in-plane variation could be quadratic or constant on the elementary domain at each interface layer.

All details about these elements are given by Bruant and Polit (2004); Polit and Bruant (2005). From these papers, the CL8EZ finite element (linear variation with respect to the thickness and constant in-plane variation) turned out to be the best compromise. Therefore, this element will be used for further comparisons in the considered benchmarks.

Main characteristics (number of mechanical dof per node, electrical dof kind and number, and in-plane electrical approximations) of finite elements picked up in literature for comparisons, are summarized in Table 1.

Apart from the element of Lam et al. (1997) and the element used in the present work, all presented piezoelectric finite elements include electrical dofs. The piezoelectric element proposed by Lam et al. is, however, a classical laminated finite element in which $\mathbf{u}_1$ and $\mathbf{u}_2$, and $\mathbf{u}_3$, are, respectively, interpolated using C^0 and C^1 functions. The piezoelectric effect is then only taken into account via external loads (thermal analogy).

In the following paragraphs, engineering notation for stresses and strains is used. The piezoelectric tensors are then the 3×6 matrices, denoted $\mathbf{d}_{ia}$, $\mathbf{e}_{ia}$, $\mathbf{g}_{ia}$, and $\mathbf{h}_{ia}$, in which a takes its values in the set $\{1, 2, 3, 4, 5, 6\}$.

Piezoelectric Data Considerations

In some of the tests presented hereafter (sections 'Laminated Composite Plate' and 'Simply Supported

Table 1. Finite element characteristics.

Characteristic	Mechanical dof per node	Electrical dof	Number of electrical dof	In-plane elect. approx.
Detwiler et al. (1995)	5	Potential	1 per interface	Constant
Suleman and Venkayya (1995)	6	Voltage	1 per layer	Constant
Lam et al. (1997)	5	None	None	Constant
Saravanos et al. (1997)	5	Potential	1 per interface ?	Linear ?
Franco Correia et al. (2000)	9	Voltage	1 per layer	Constant
Fukunaga et al. (2001)	7	Voltage	1 per layer	Constant
Cen et al. (2002)	5	Potential	1 per node of interface	Bilinear
CL8EZ (Bruant and Polit, 2004)	5	Potential	1 per interface	Constant
Present work	5	None	None	Constant

Square Plate'), some piezoelectric properties have to be modified.

In particular, the piezoelectric constants $\mathbf{d}_{3\alpha}$ and $\mathbf{d}_{33}$ provided in these tests are of similar sign. The isolated stiffness and compliance matrices can be evaluated by using Equations (24) in the companion paper (Osmont and Pablo, 2008) and the original data. This leads to negative determinants, i.e., these matrices are not positive-defined ones, which is not consistent with mechanical theories. Moreover, piezoelectric materials do not have the ability of volume expansion when they are subjected to a transverse electric field ($\mathbf{E}_3$), which would be obtained by the original data: $\mathbf{d}_{3\alpha}$ and $\mathbf{d}_{33}$ must have opposite signs. Since classical piezoelectric materials used as actuators are characterized by negative $\mathbf{d}_{3\alpha}$ and positive $\mathbf{d}_{33}$, this sign agreement is used hereafter.

The modifications brought to the piezoelectric constants do not have any drawbacks on the solution. This point can easily be proved. Let us consider the last test presented in this article (section 'Simply Supported Square Plate'), in which the sign of $\mathbf{d}_{33}$ has been changed to positive. Calculating, for example, the $\mathbf{e}_{31}$ piezoelectric coefficient ($\mathbf{e} = \mathbf{d}\mathbb{C}^E$) using the data of Saravanos et al. (1997), one obtains $\mathbf{e}_{31}^{literature} \approx -47.3242\,\mathrm{C/m^2}$. Using the data used in the present article, this value is $\mathbf{e}_{31}^{Pablo} \approx -5.34795\,\mathrm{C/m^2}$. Now, developing plate models, plane stress assumption is generally used. This assumption induces significant modifications in the matrices of piezoelectric coefficients $\mathbf{d}$ and $\mathbf{e}$. Considering our example, $\mathbf{e}_{31}$ becomes $\bar{\mathbf{e}}_{31} = \mathbf{e}_{31} - (\mathbb{C}_{13}/\mathbb{C}_{33})\mathbf{e}_{33}$. Calculating this 'plane stress' coefficient in the two cases, one respectively obtains $\bar{\mathbf{e}}_{31}^{literature} \approx -14.8039\,\mathrm{C/m^2}$ and $\bar{\mathbf{e}}_{31}^{Pablo} \approx -14.8039\,\mathrm{C/m^2}$. Thus, the modification brought to $\mathbf{d}_{33}$ sign is cancelled by the plane stress assumption. This conclusion can be expanded to other tests and other piezoelectric constants through similar developments.

Static Tests

Three benchmarks available in open literature are hereafter examined in order to evaluate the present finite element approach to different plates under static loads.

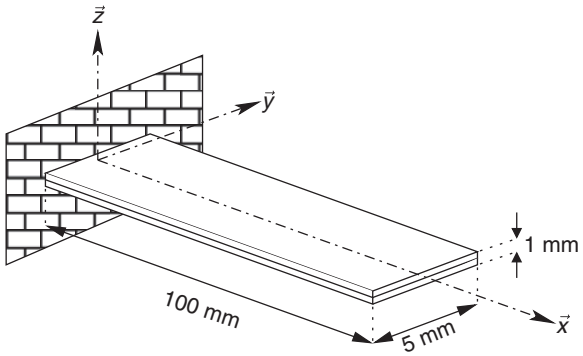

Figure 1. Piezoelectric bimorph beam.

Table 2. PVDF mechanical and piezoelectric properties.

Mechanical properties			Piezoelectric properties		
E_i	$G_{12} = G_{13} = G_{23}$	ν_{ij}	$\mathbf{e}_{31} = \mathbf{e}_{32}$	$\mathbf{e}_{33}$	ε_{33}^S
2 GPa	1 GPa	0	0.046 C/m^2	0 C/m^2	0.1062 nF/m

PIEZOELECTRIC BIMORPH BEAM

The first numerical validation is based on an experiment conducted by Tzou et al. (1990). The present experiment has been widely used in literature to validate finite elements (Detwiler et al., 1995; Suleman and Venkayya, 1995; Franco Correia et al., 2000; Fukunaga et al., 2001; Cen et al., 2002; Bruant and Polit, 2004).

A cantilever piezoelectric beam made of two piezoelectric polymeric PVDF layers with opposite polarity is considered. The lower and upper faces of the beam are subjected to a 1V electric potential and the mid-line beam deflection is measured.

The beam geometrical specifications and the PVDF mechanical and piezoelectric properties provided by the authors (Tzou et al., 1990) are presented in Figure 1 and Table 2, respectively.

In the present work, the beam is discretized using a regular mesh composed of five elements. The isolated

Table 3. Nodal deflection of the bimorph piezoelectric beam (μm).

Distance from clamping (mm)	20	40	60	80	100
Experiment (Tzou et al., 1990)	–	–	–	–	0.315
Detwiler et al. (1995)	0.014	0.055	0.210	0.221	0.345
Suleman and Venkayya (1995)	0.014	0.055	0.124	0.221	0.345
Franco Correia et al. (2000)	0.013	0.051	0.114	0.202	0.316
Fukunaga et al. (2001)	0.0139	0.0553	0.124	0.221	0.345
Cen et al. (2002)	0.0138	0.0552	0.1242	0.2208	0.3450
CL8EZ (Bruant and Polit, 2004)	0.0137	0.0551	0.1241	0.2207	0.3449
Present work	0.0137	0.0549	0.1235	0.2197	0.3433

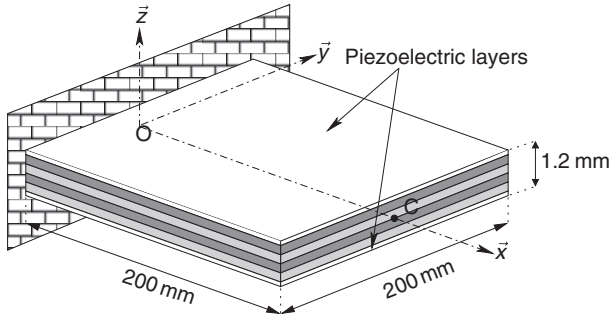

Figure 2. *Cantilever laminated composite plate.*

and short-circuited mechanical and piezoelectric matrices needed in the present theory are obtained using relationships (24) presented in Osmont and Pablo (2008).

Table 3 compares the results obtained by the present theory with those provided in literature.

The present theory leads to similar results to those found in literature. The error, in comparison with the experimental tip displacement, is then ~9%. It is to be noticed that the results obtained by Franco Correia et al. are very close to the experimental tip deflection (error is ~0.3%). On the other hand, present results are <0.5 % different from nodal deflections given in other references (Detwiler et al., 1995; Suleman and Venkayya, 1995; Fukunaga et al., 2001; Cen et al., 2002; Bruant and Polit, 2004).

LAMINATED COMPOSITE PLATE

This second test is proposed by Lam et al. (1997). It consists in a 200×200 mm^2 square cantilever laminated composite plate made of six homogeneous layers: two 0.1 mm thick PZT G1195N piezoelectric layers and four 0.25 mm thick T300/976 graphite-epoxy composite layers. The stacking sequence used to elaborate the composite plate is [piezo/$-\theta/\theta/-\theta/\theta$/piezo] in which $\theta = 45^\circ$ is the longitudinal direction of each composite ply with respect to the $O\vec{x}$ axis (Figure 2).

The material properties used by Lam et al. (1997), were previously given by Ha et al. (1992) and are summarized in Table 4.

Table 4. Materials properties.

	PZT G1195N	T300/976 composite
Young's moduli (GPa):		
E_1	63.0	150.0
$E_2 = E_3$	63.0	9.0
Poisson's ratio:		
$\nu_{12} = \nu_{13}$	0.3	0.3
$\nu_{32} = \nu_{23}$	0.3	0.3
Shear moduli (GPa):		
$G_{12} = G_{13}$	24.2	7.1
G_{23}	24.2	2.5
Density (kgm^{-3}):		
ρ	7600.0	1600.0
Piezoelectric constants (pmV^{-1}):		
$\mathbf{d}_{31} = \mathbf{d}_{32}$	−254.0	–
$\mathbf{d}_{15} = \mathbf{d}_{24}$	584.0	–
$\mathbf{d}_{33}$	374.0	–
Electrical permittivity (nFm^{-1}):		
$\varepsilon_{11}^T = \varepsilon_{22}^T$	15.3	–
ε_{33}^T	15.0	–

According to the discussion in the section 'Piezoelectric Data Considerations', the signs of the piezoelectric constants $\mathbf{d}_{31}$ and $\mathbf{d}_{32}$ have been taken negative in contrast to Ha et al. (1992) data. Two numerical simulations are presented hereafter:

(1) Actuator application. The laminated plate is free from any mechanical load and subjected to an electrical load: electrical potentials with similar magnitudes but opposite sign are, respectively, applied on the upper (positive) and lower (negative) faces of the plate. Voltage magnitudes ranging from 0 to 60 V have been used. The plate deflection is calculated using the present theory and compared to results obtained by Lam et al. (1997).
(2) The results presented in Figure 3 have been obtained using a 36 finite element mesh which is similar to that employed by Lam et al. Figure 3(a) represents the deflection of the plate midsurface under a 10 V static electric potential load, and, in Figure 3(b) the plate centerline's free end tip deflection (point C) is plotted as a function of various electric potentials.
(3) Static counteraction. A 100 Nm^{-2} uniform pressure is applied on the upper face of the plate,

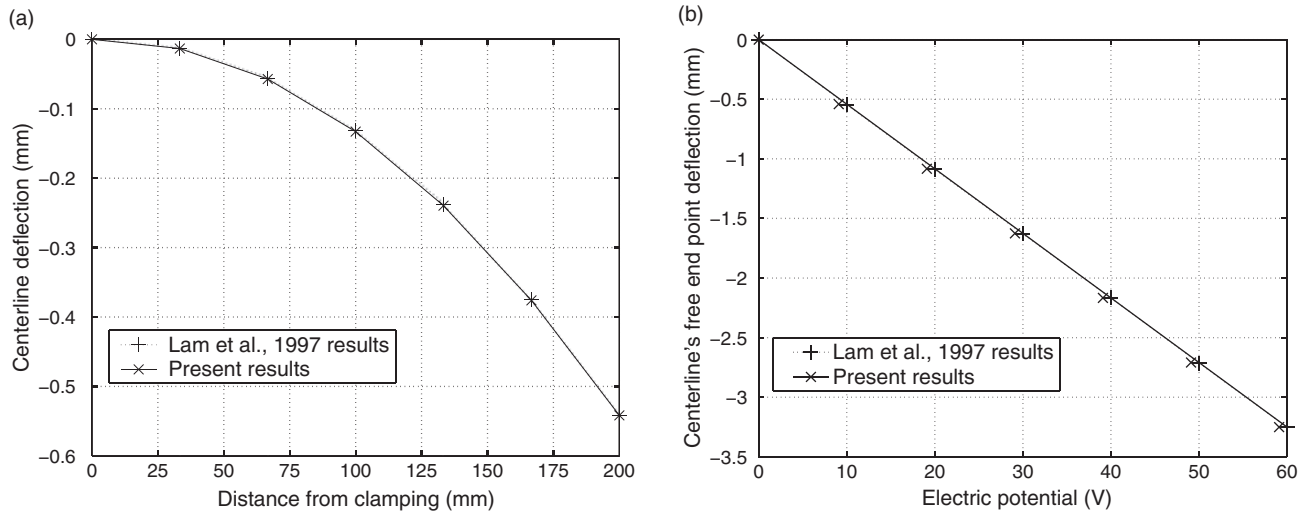

Figure 3. *Plate centerline deflection under electrical loads.*

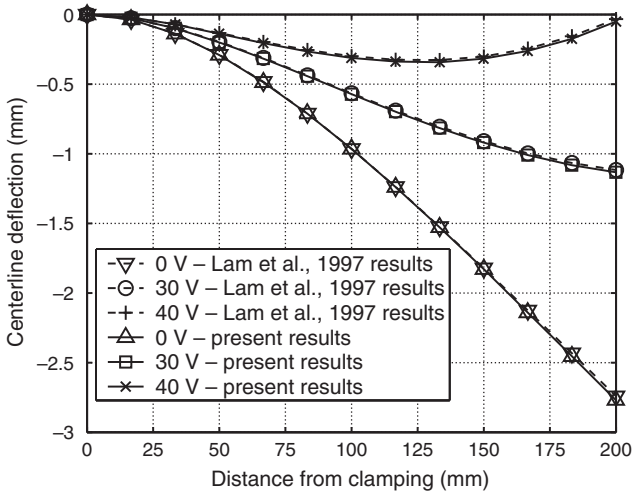

Figure 4. *Input voltage effect on the flatten plate.*

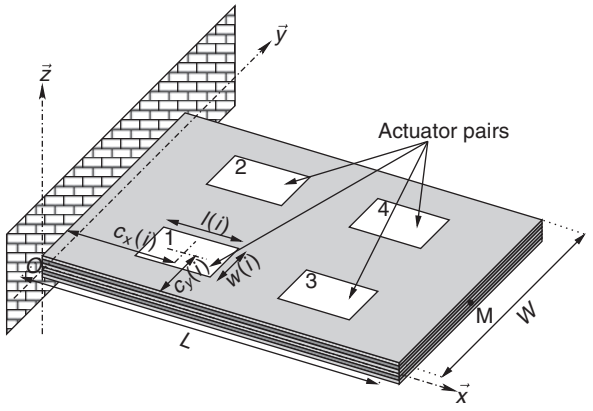

Figure 5. *Active composite plate.*

inducing bending. A static potential with opposite signs is then gradually applied to the piezoelectric actuators in order to reduce centerline deflection. Results obtained with the present theory are compared to those of Lam et al. in Figure 4.

For all considered cases the curves are found to coincide. Nevertheless, Figure 4 shows that the present approach slightly softens the plate behavior. This difference is due to the modifications applied to the elastic coefficients of piezoelectric materials in the present theory.

Based on these results, the present theory is consistent with laminated composite plates including piezoelectric layers, each layer being continuous in plane.

ACTIVE PLATE

The last static test is inspired from Franco Correia et al. (2000) and Polit et al. (Bruant and Polit, 2004).

A cantilever rectangular composite plate equipped with four rectangular piezoelectric actuator pairs is studied.

For the present test, the piezoelectric material proposed in the original one (Franco Correia et al., 2000) could not be used. Indeed, piezoelectric properties provided by the authors are not complete (missing piezoelectric constants and electrical permittivity). As a consequence, the electromechanical matrices needed in the present theory could not be evaluated. The PZT4 piezoelectric material proposed by Saravanos et al. (1997) will thus be used in the test proposed hereafter.

The plate is made of six 0.508 mm thick graphite/Epoxy composite layers, with a $[90°/0°/90°]_s$ stacking sequence. This composite plate is $L = 240$ mm long and $W = 120$ mm wide, and is clamped along the $O\vec{y}\vec{z}$ plane as presented in Figure 5.

Each actuator pair (with opposite polarization) is supposed to be perfectly and symmetrically bonded on the lower and upper faces of the composite plate.

Table 5. Materials properties.

	PZT-4	Graphite/Epoxy
Young's moduli (GPa):		
E_1	81.3	97.974
E_2	81.3	7.9
E_3	64.5	7.9
Poisson's ratio:		
ν_{12}	0.33	0.28
$\nu_{13} = \nu_{23}$	0.43	0.28
Shear moduli (GPa):		
G_{12}	30.6	5.5999
$G_{13} = G_{23}$	25.6	5.5999
Density (kgm^{-3}):		
ρ	7600.0	Not given
Piezoelectric constants (pmV^{-1}):		
$\mathbf{d}_{31} = \mathbf{d}_{32}$	−122.0	–
$\mathbf{d}_{15} = \mathbf{d}_{24}$	0	–
$\mathbf{d}_{33}$	285.0	–
Electrical permittivity (nFm^{-1}):		
$\varepsilon_{11}^T = \varepsilon_{22}^T$	13.05	–
ε_{33}^T	11.51	–

Table 6. Nodal deflection and rotation at point M.

	w (mm)	θ_x (10^{-2} rad)
CL8EZ	−0.32863	−0.28015
Present work	−0.32856	−0.28012

The aim of this test is to evaluate the active control of composite plates and thus to evaluate the influence of the piezoelectric patch dimensions and locations. As a consequence, patch sizes and positions are changing. The ith ($i = 1, \ldots, 4$) piezoelectric pair is thus supposed to be $l(i)$ mm long, $w(i)$ mm wide and $t(i)$ mm thick, and, its geometric center is supposed to be placed at $c_x(i)$ mm and $c_y(i)$ mm in the $O\vec{x}\vec{y}$ axis.

In this particular static test all patches are assumed to be 60 mm long, 30 mm wide, and 0.254 mm thick and the following statements are used: $c_x(1) = c_x(2) = 60\,\text{mm}$, $c_x(3) = c_x(4) = 180\,\text{mm}$, $c_y(1) = c_y(3) = 30\,\text{mm}$, and $c_y(2) = c_y(4) = 90\,\text{mm}$.

Materials properties used in this numerical application are summarized in Table 5 (the PZT-4 and Graphite/Epoxy properties were respectively given by Saravanos et al. (1997) and Franco Correia et al. (2000)).

For physical reasons (see explanation in section 'Piezoelectric Data Considerations') the $\mathbf{d}_{33}$ sign has been changed to positive compared to Saravanos et al. data (1997).

In this test, a 300 V static electric potential is applied to each actuator, the deflection w and the rotation θ_x at point M ($x = L$, $y = W/2$, 0) are recorded. Table 6 presents results obtained using our theory, and using the CL8EZ piezoelectric finite element (Bruant and Polit, 2004) with a 8×8 mesh.

The differences between the two finite elements are, respectively, ~0.2 and 0.1% for the nodal deflection and the rotation. The present theory is thus consistent with laminated composite plates equipped with distributed actuators (non-continuous layers in plane).

Table 7. Calculated natural frequencies (Hz).

Natural frequencies	Lam et al.	Present work	Difference (%)
1	21.4657	21.513	0.22
2	63.3491	63.250	0.16
3	130.8221	129.700	0.86
4	182.4224	182.950	0.29
5	218.2750	217.600	0.31
6	381.9788	377.470	1.18
7	395.7263	400.150	1.12
8	410.9160	409.680	0.30
9	476.4277	475.120	0.27
10	642.9230	658.200	2.38

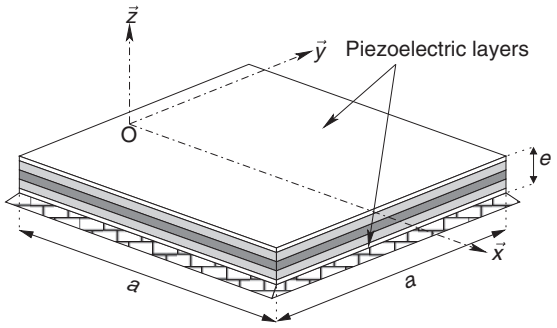

Figure 6. *Simply supported laminated composite plate.*

Frequency Tests

This theory has been validated for static electromechanical loads. Two benchmarks are hereafter proposed from literature for frequency validations.

CANTILEVER COMPOSITE PLATE

The first test, proposed by Lam et al. (1997), is based on the geometry and the material properties described in section 'Laminated Composite Plate', and presented in Figure 2.

In the present test, the piezoelectric layers are short-circuited (0 V electric potential). The first 10 natural frequencies are calculated and compared to those obtained by Lam et al. (1997) in Table 7.

One can observe that the greater difference between the two theories is <2.5%.

The present theory is thus consistent with frequency analysis of laminated plates containing short-circuited piezoelectric layers.

SIMPLY SUPPORTED SQUARE PLATE

The test proposed by Saravanos et al. (1997) and successively used by Franco Correia et al. (2000) and Polit et al. (Bruant and Polit, 2004) is examined.

The free-vibration response of a square simply-supported laminated composite plate is analyzed (Figure 6). The plate is made of three Graphite/Epoxy composite layers and two piezoelectric layers according to a [piezo/0°/90°/0°/piezo] stacking sequence.

The edge length of the square plate is denoted by a (m) and its thickness by c (m). The thickness of the piezoelectric and graphite/epoxy layers are $0.1 \times e$ m, and $0.267 \times e$ m, respectively. The material properties used in this test are given in Table 8, in which the $\mathbf{d}_{33}$ sign has been changed to positive for physical reasons (see explanation in section 'Piezoelectric Data Considerations').

Table 8. Materials properties.

	PZT-4	Graphite/Epoxy
Young's moduli (GPa):		
E_1	81.3	132.38
E_2	81.3	10.76
E_3	64.5	10.76
Poisson's ratios:		
ν_{12}	0.33	0.24
ν_{13}	0.43	0.24
ν_{23}	0.43	0.49
Shear moduli (GPa):		
G_{12}	30.6	5.65
G_{13}	25.6	5.65
G_{23}	25.6	3.61
Density (kgm^{-3}):		
ρ	7600.0	1578
Piezoelectric constants (pmV^{-1}):		
$\mathbf{d}_{31} = \mathbf{d}_{32}$	−122.0	–
$\mathbf{d}_{15} = \mathbf{d}_{24}$	0	–
$\mathbf{d}_{33}$	285.0	–
Electrical permittivity (nFm^{-1}):		
$\varepsilon_{11}^T = \varepsilon_{22}^T$	13.05	–
ε_{33}^T	11.51	–

While the outer surfaces of the piezoelectric layers are enforced to remain grounded ($V = 0$), two different electric boundary conditions are defined for the inner interfaces (Saravanos et al., 1997):

(1) the short-circuited boundary condition is obtained by enforcing the inner surfaces of the piezoelectric layers to be grounded ($V = 0$),
(2) the 'isolated' boundary condition is obtained by keeping the electric potential free on the inner surfaces of the piezoelectric layers.

It is to be noticed that quotation marks have been used for the word *isolated* because a real isolated boundary condition should enforce the electric displacements to be zero ($D_z = 0$) on the two surfaces of the piezoelectric layers. Since the model of Saravanos et al. has been developed as a function of the electric potentials, electrical boundary conditions involving electric displacements can not be imposed. To overcome this difficulty the present work implements various models corresponding to different electrical boundary conditions (Equations (1)–(4)). In the present test, the isolated boundary condition thus corresponds to $Q_l^i = Q_u^i = 0$.

The numerical simulation is conducted using an 8×8 mesh. The unit mass density is assumed for all the layers ($\rho = 1\,kg/m^3$) in order to compare the results with the analytical solutions of Heyliger and Saravanos (1989).

The first five frequencies obtained with the present theory are compared to other results found in literature (Table 9):

- a three dimensional layerwise exact solution from Heyliger and Saravanos (1989),

Table 9. First five non-dimensionalized frequencies $\tilde{f}_i$.

Frequency (10^3 Hz$\sqrt{m/kg}$)		$\tilde{f}_1$	$\tilde{f}_2$	$\tilde{f}_3$	$\tilde{f}_4$	$\tilde{f}_5$
No piezoelectric effect (purely mechanical):						
CL8 (LMpX)		233.325	526.450	671.400	926.700	1033.175
Short-circuited boundary conditions:						
Heyliger et al. (Heyliger and Saravanos, 1989)	(a)	245.941	–	–	–	–
Saravanos et al. (1997)	(b)	237.109	–	–	–	–
Correia et al. (2000)	(c)	206.304	519.444	663.336	907.636	1020.102
Benjeddou et al. (2002)	(a)	246.067	559.615	693.601	967.141	1091.458
CL8EZ (Polit and Bruant, 2005)	(a)	246.462	560.725	698.300	973.925	1097.175
CL8EZ new	(b)	233.295	552.637	671.350	926.575	1033.050
Present work	(b)	233.405	526.700	671.475	927.000	1033.675
Isolated boundary conditions:						
Heyliger et al. (Heyliger and Saravanos, 1989)	(i)	245.942	–	–	–	–
Saravanos et al. (1997)	(ii)	259.895	–	–	–	–
Correia et al. (2000)	(iii)	245.349	558.988	694.196	962.017	1093.006
Benjeddou et al. (2002)	(i)	246.068	559.621	693.606	967.155	1091.481
CL8EZ (Polit and Bruant, 2005)	(iv)	246.462	560.725	698.300	973.925	1097.175
Present work	(v)	255.825	587.375	719.400	1014.275	1154.400

- a finite element solution based on layerwise laminate theories from Saravanos et al. (1997),
- a finite element solution based on a higher order displacement model (Q9-FSTD) from Franco Correia et al. (2000),
- a 2D closed-form solution from Benjeddou et al. (2002),
- a finite element solution using CL8EZ model from Polit et al. (Polit and Bruant, 2005)
- a finite element solution using CL8EZ with modified short-circuited boundary conditions.

These frequencies are non-dimensionalized using the following relationship:

$$\tilde{f}_i = f_i \frac{a^2}{e\sqrt{\rho}}.$$

Considering the first frequency, Benjeddou et al. (2002) and Polit et al. (Polit and Bruant, 2005) models are closer to the Heyliger et al. exact solution than the present theory in both cases. On the other hand, the present theory leads to results which are similar to those presented by Saravanos et al. (1997) and Franco Correia et al. (2000) and to new ones obtained using the CL8EZ model. Indeed, these last results reveal significant differences (about 10 %) between the short-circuited and isolated natural frequencies.

An analysis of electric boundary conditions used in literature is now essential in order to correctly analyze the results presented in Table 9.

First, three 'short-circuited' boundary conditions can be distinguished:

(a) The electric potentials are enforced to be zero on the outer surfaces of the piezoelectric layers, while they remain free on their inner surfaces Figure 7(a). These boundary conditions were used by Benjeddou et al. (2002), Polit et al. (Polit and Bruant, 2005), and probably Heyliger and Saravanos (1989).
(b) The electric potentials are enforced to be zero on the inner and outer surfaces of the piezoelectric layers Figure 7(b). These boundary conditions were used by Saravanos et al. (1997), in the present work, and for the new CL8EZ results.
(c) The voltages are enforced to be zero through the thickness of the piezoelectric layers Figure 7(c). These boundary conditions were used by Franco Correia et al. (2000).

Furthermore, five 'isolated' boundary conditions can be distinguished:

(i) The electric potentials remain free on the inner and outer surfaces of the piezoelectric layers Figure 8(a). These boundary conditions were used by Benjeddou et al. (2002) and probably Heyliger and Saravanos (1989).
(ii) The electric potentials are enforced to be zero on the outer surfaces of the piezoelectric layers, while they remain free on their inner surfaces Figure 8(b). These boundary conditions were used by Saravanos et al. (1997).

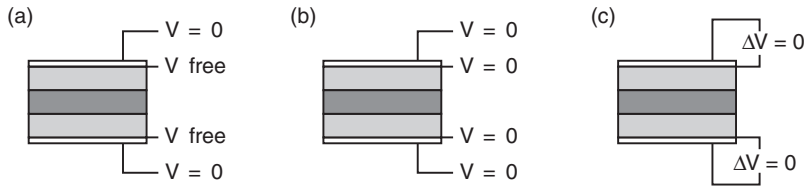

Figure 7. *Short-circuited (closed-circuit) boundary conditions.*

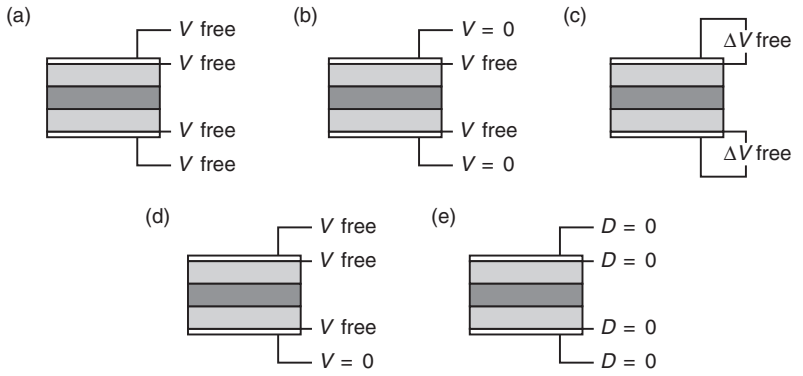

Figure 8. *Isolated (open-circuit) boundary conditions.*

(iii) The voltages remain free through the thickness of the piezoelectric layers Figure 8(c). These boundary conditions were used by Franco Correia et al. (2000).
(iv) The electric potentials remain free everywhere, except on the bottom surface of the plate where it is enforced to be zero Figure 8(d). These boundary conditions were used by the CL8EZ element of Polit et al. (Polit and Bruant, 2005).
(v) The electric charges are enforced to be zero on the inner and outer surfaces of the piezoelectric layers Figure 8(e). These boundary conditions have been used in the present work.

It is first surprising to notice that identical boundary conditions have been defined as 'short-circuited' Figure 7(a) and isolated Figure 8(b). Physically, a piezoelectric plate is short-circuited when its opposite faces are at the same electric potentials. This boundary condition corresponds to case (b) described above. If the potential remains free on one of the two faces, the piezoelectric layer is not strictly short-circuited. Thus, 'closed-circuit' values given by Benjeddou et al. (2002), Polit et al. (Polit and Bruant, 2005), and probably Heyliger and Saravanos (1989) can not be considered as a reference for the present work.

Comparing the mechanical and short-circuited natural frequencies obtained with physical boundary conditions, one can note two cases:

(1) The natural frequencies obtained by Saravanos et al. (1997) and in the present work are higher than the purely mechanical ones,
(2) Those obtained by Correia et al. (2000) as well as those extracted with the CL8EZ finite element (Polit and Bruant, 2005) are lower than the purely mechanical ones.

Furthermore, the first short-circuited frequency obtained by Franco Correia et al. (2000) is very different from the mechanical one (~12%). This result is quite surprising since in all other cases this difference is, at most, of ~2%.

Now, the plate bending induces electric charges which modify the stiffness of the piezoelectric layers. Indeed, the constitutive laws for short-circuited piezoelectric layers are:

$$\mathbf{T} = \mathbb{C}^E \mathbf{S} - {}^t\mathbb{e}\,\mathbf{E} \tag{15}$$

$$\mathbf{D} = \mathbb{e}\,\mathbf{S} + \varepsilon^S \mathbf{E}. \tag{16}$$

Inverting Equation (16) one can express the electric field $\mathbf{E}$ as a function of strain $\mathbf{S}$ and electric displacement $\mathbf{D}$. Replacing this value in Equation (15) one obtains the following stresses:

$$\mathbf{T} = (\mathbb{C}^E + {}^t\mathbb{e}\,\beta^S\,\mathbb{e})\mathbf{S} + \beta^S\,\mathbb{e}\,\mathbf{D} = (\mathbb{C}^E + \mathbb{C}^E_{piez})\mathbf{S} + \beta^S\,\mathbb{e}\,\mathbf{D}.$$

Now, assuming plane stress conditions, the additional stiffness contribution $\overline{\mathbb{C}}^E_{piez}$ is either positive or zero. Therefore, the bending of the plate should induce an increase in the stiffness of the piezoelectric layer. As a consequence, the short-circuited natural frequencies can not be smaller than the mechanical ones. This is consistent with the results obtained by Saravanos et al. (1997) and by the present theory.

Let us now focus our interest on 'isolated' results. One can observe that four sets of results are similar: Heyliger and Saravanos (1989), Franco Correia et al. (2000), Benjeddou et al. (2002) and CL8EZ (Polit and Bruant, 2005) ones. This indicates that the 'isolated' boundary conditions (i), (iii), and (iv) can be interpreted to be nearly equivalent. Moreover short-circuited natural frequencies obtained using (a) boundary conditions are very close, or equal, to isolated natural frequencies. Therefore, it seems that boundary conditions (a) are in fact isolated ones. As a consequence, setting at least one potential to be free seems to correspond to isolated boundary condition.

Finally results obtained using the present theory are quite different from the previous ones. Only two explanations can be proposed for these variations:

- either the (i), (iii), and (iv) electric boundary conditions are not similar to realistic isolated ones,
- or isolated frequencies are overestimated in the present theory.

The point is being considered.

CONCLUSION

An original theory for multilayered plate structures including piezoelectric patches was proposed in the first part of this article. This theory is based on *a priori* plate assumptions and leads to the suppression of the electric variables from the problem unknowns. The electromechanical effect is then taken into account *via* the modification of the stiffness coefficients and the addition of a piezoelectric load, depending on electric boundary conditions, to the second member. Different electrical boundary conditions for each piezoelectric layer have been implemented. Classical plate finite elements can be then used to simulate the behavior of piezoelectric laminate under static or dynamic loads.

The present theory has been implemented and validated through benchmarks taken from literature. The stiffness and mass matrices remaining symmetrical, classical resolution schemes can be used in this method.

For static electromechanical loads, results obtained by the present theory are <5% different from the reference numerical results available in literature.

The simply supported frequency test reveals that the electric boundary conditions (short-circuited or isolated) induce a nonnegligible variation of natural frequencies. Moreover, the possibility of correctly taking into account isolated boundary conditions in a 'potential' based model has been investigated. It seems that setting at least one potential to be free corresponds to this electric boundary condition.

On the other hand, in the two tests presented here, the natural frequencies obtained by the present theory are $<5\%$ different compared to the ones found in literature. The present theory can thus be used for active vibration control analyses.

A drawback of the present theory lies in the fact that the electromechanical properties of the piezoelectric material have to be fully known so as to be able to estimate the required matrices. These properties being often partially given in literature, comparisons with other theories are often impossible.

Calculation time was compared within the LMpX in the last test presented above. It stands out that the present theory is about four times faster than CL8EZ finite element (Polit and Bruant, 2005), which is a real advantage.

In the present article, tests have been carried out for piezoelectric layers being actuators (applied electric potentials). A subsequent work should focus on showing the efficiency of the present theory for active vibration control applications.

Finally, the present theory has been developed with the view of performing active vibration control simulations. The differences between the present results and those presented in literature being $<5\%$, the present theory is suitable for such applications.

REFERENCES

Benjeddou, A., Deu, J.F. and Letombe, S. 2002. "Free Vibrations of Simply-supported Piezoelectric Adaptive Plates: An Exact Sandwich Formulation," *Thin-walled Structures*, 40:573–593.

Bruant, I. and Polit, P. 2004. "A New Piezoelectric 8 Node Finite Element Family for Active Control," *Hellenic European Research on Mathematics and Informatics Science*, 5:25–37.

Cen, S., Soh, A.-K., Long, Y.-Q. and Yao, Z.-H. 2002. "A New 4-node Quadrilateral fe Model with Variable Elelctrical Degrees of Freedom for the Analysis of Piezoelectric Laminated Composite Plates," *Composite Structures*, 58:583–599.

Detwiler, D.T., Shen, M.-H.H. and Venkayya, V.B. 1995. "Finite Element Analysis of Laminated Composite Structures Containing Distributed Piezoelectric Actuators and Sensors," *Finite Elements in Analysis and Design*, 20:87–100.

Franco Correia, V.M., Aguiar Gomes, M.A., Suleman, A., Mota Soares, C.M. and Mota Soares, C.A. 2000. "Modelling and Design of Adaptive Composite Structures," *Computer Methods in Apllied Mechanics and Engineering*, 185:325–346.

Fukunaga, H., Hu, N. and Ren, G.X. 2001. "Fem Modeling of Adaptive Composite Structures Using a Reduced Higher-order Plate Theory via Penalty Functions," *IJSS*, 38:8735–8752.

Ganapathi, M., Polit, O. and Touratier, M. 1996. "A c^0 Eight-node Membrane-shear-bending Element for Geometrically Non-linear (Static and Dynamic) Analysis of Laminates," *International Journal for Numerical Methods in Engineering*, 39:3453–3474.

Ha, S.K., Keilers, C. and Chang, F. 1992. "Finite Element Analysis of Composite Structures Containing Distributed Piezoceramic Sensors and Actuators," *American Institute of Aeronautics and Astronautics Journal*, 30(3):772–780.

Heyliger, P. and Saravanos, D.A. 1989. "Exact Free-vibration Analysis of Laminated Plates with Embedded Piezoelectric Layers," *Journal of the Acoustical Society of America*, 98(3): 1547–1556.

Ikeda, T. 1990. *Fundamentals of Piezoelectricity*, Oxford University, Oxford.

Lam, K.Y., Peng, X.Q., Liu, G.R. and Reddy, J.N. 1997. "A Finite-element Model for Piezoelectric Composite Laminates," *Smart Materials and Structures*, 6:583–591.

Osmont, D. and Pablo, F. 2009. "Use of Classical Plate Finite Elements for Analysis of Electroactive Composite Plates. Theoretical Aspects," *Journal of Intelligent Materials, Systems and Structures*, DOI: 10.1177/1045389X09337082.

Polit, O. and Bruant, I. 2005. "Electric Potential Approximations for an Eight Node Plate Finite Element," *Computers and Structures*, 84:1480–1493.

Polit, O., Touratier, M. and Lory, P. 1994. "A New Eight-node Quadrilateral Shear-bending Plate Finite Element," *International Journal for Numerical Methods in Engineering*, 37:387–411.

Preumont, A. 1997. *Vibration Control of Active Structures*, Kluwer Academic Publishers, Dordrecht, The Netherlands.

Saravanos, D.A., Heyliger, P.R. and Hopkins, D.A. 1997. "Layerwise Mechanics and Finite Element for the Dynamic Analysis of Piezoelectric Composite Plates," *International Journal of Solids and Structures*, 34(3):359–378.

Suleman, A. and Venkayya, V.B. 1995. "A Simple Finite Element Formulation for Laminated Composite Plate with Piezoelectric Layers," *Journal of Intelligent Materials, Systems and Structures*, 6:776–782.

Tzou, H.S., Tseng, C.I. and Wan, G.C. 1990. "Distributed Structural Dynamics Control of Flexible Manipulators-II. Distributed Sensor and Active Electromechanical Actuator," *Computers and Structures*, 35(6):679–687.